Available online at www.sciencedirect.com
ScienceDirect
Thin Solid Films 516 (2008) 3948–3956
www.elsevier.com/locate/tsf

Study of self-assembled triethoxysilane thin films made by casting neat reagents in ambient atmosphere

Yongan Yang [a,*], Alexander M. Bittner [a,*], Steve Baldelli [b], Klaus Kern [a]

[a] Max Planck Institute for Solid State Research, Stuttgart, Germany
[b] University of Houston, Department of Chemistry, Houston TX, USA

Received 24 December 2006; received in revised form 27 July 2007; accepted 27 July 2007
Available online 11 August 2007

Abstract

We studied four trialkoxysilane thin films, fabricated *via* self-assembly by casting neat silane reagents onto hydrophilic SiO_x/Si substrates in the ambient. This drop-casting method is simple, yet rarely studied for the production of silane self-assembled monolayers (SAMs). Various *ex-situ* techniques were utilized to systematically characterize the growth process: Ellipsometry measurements can monitor the evolution of film thickness with silanization time; water droplet contact angle measurements reveal the wettability; the change of surface morphology was followed by Atomic Force Microscopy; the chemical identity of the films was verified by Infrared–Visible Sum Frequency Generation spectroscopy. We show that the shorter carbon chain (propyl-) or branched (2-(diphenylphosphino)ethyl-) silane SAMs exhibit poor ordering. In contrast, longer carbon chain (octadecyl and decyl) silanes form relatively ordered monolayers. The growth of the latter two cases shows Langmuir-like kinetics and a transition process from lying-down to standing-up geometry with increasing coverage.

Keywords: Self-assembly; Silane; Atomic force microscopy; Water contact angle; Ellipsometry; Sum frequency generation

1. Introduction

Silanes have been extensively studied as they can form robust self-assembled monolayers (SAMs) due to covalent siloxane bonds between the molecules and hydroxyl-terminated substrates [1]. One end of the silane molecules features one or more reactive bonds, such as Si–OR or Si–Cl. In the presence of water or OH groups on the surface, they can hydrolyze to form covalent bonds Si–O-substrate. Intrinsically, alkoxysilanes and chlorosilanes do not show significant differences, considering the final structure of the corresponding SAMs. Alkoxysilanes are more stable and easy to control under ambient conditions, while chlorosilanes are very susceptible to humidity [2]. Trialkoxysilane SAMs contain intermolecular networks with lateral Si–O-Si bonds [3], although steric constraints do not allow a perfectly ordered two-dimensional network [4]. At the other end of the silane molecules, various functional groups can be designed according to specific purposes, like CH_3 and CF_3 for lubrication and hydrophobicity [5,6], CH═CH_2, COOH and OH for binding to application surfaces [3,7,8], (*e.g.*, for chromatography [9]), NH_2, SH, and PPh_2 for immobilizing metal nanoparticles [10–14]. The carbon chain length can also be changed to tune the SAM properties [15]. Based on these considerations, many important applications for silane SAMs have been proposed and investigated, such as biomolecular anchoring and sensoring [16,17], catalysis by immobilizing metal nanoparticles [12,14], and build-up of molecular transistors [18].

Since silane SAMs have so many intriguing applications, their fabrication becomes naturally important. Two preparation methods have been widely studied. One is to immerse clean substrates in a solution of a target silane reagent for a specified time, here called the “Solution Method” (SM) [2,3,12]. One may deliberately introduce water traces to study its influence [19–21]; more often, water from the ambient (humid atmosphere) suffices to induce and/or speed up hydrolysis. Too much water can actually cause aggregation of silane molecules and induce fractal structures and low-quality SAMs [20]. Another

* Corresponding authors. Yang is to be contacted at Present address: University of California, Irvine, Department of Chemistry, Irvine CA, USA. Tel.: +1 949 824 6178.
E-mail addresses: yongany@uci.edu (Y. Yang), a.bittner@fkf.mpg.de (A.M. Bittner).

0040-6090/$ - see front matter © 2007 Elsevier B.V. All rights reserved.
doi:10.1016/j.tsf.2007.07.208

common method is the exposure of clean substrates to silane vapor in vacuum with or without heating, termed "Vapor Method" (VM) [22–24]. In a good vacuum, a very limited water supply is available, and the resulting SAMs might not show full coverage [23]. The third method, directly casting of neat silanes (Casting Method, CM), which was initially performed on hot substrates [8,25], was rarely studied in detail. As yet, thorough structural and chemical characterizations for CM-produced silane films are not available. Here we report a systematic study on various silane films, produced from OTS (octadecyltriethoxysilane), DTS (decyltriethoxysilane), PTS (propyltriethoxysilane) and DPES (2-(diphenylphosphino)-ethyltriethoxysilane), and characterized by ellipsometry, contact angle measurements, atomic force microscopy (AFM) and sum frequency generation (SFG).

2. Experimental details

2.1. Chemical reagents

All silanes, OTS (Octadecyltriethoxysilane, $CH_3(CH_2)_{17}Si(OEt)_3$), DTS (Decyltriethoxysilane, 97%, $CH_3(CH_2)_9Si(OEt)_3$), PTS (Propyltriethoxysilane, 98%, $CH_3(CH_2)_2Si(OEt)_3$) and DPES (2-(diphenylphosphino)ethyltriethoxysilane, 97%, $Ph_2P(CH_2)_2Si(OEt)_3$) were from ABCR (Karlsruhe, Germany) and used without further treatment. Absolute ethanol (>99.9%) was from J. T. Baker, Holland. Acetone (p.a., >99.5%) was from Carl Roth (Karlsruhe, Germany). Suprapur HCl solution (30%), VLSI selectipur H_2O_2 solution (31%) and NH_4OH solution (25%) were all from Merck. Millipore water with a specific resistance of 18.2 MΩ was used.

2.2. Substrate pretreatment

Si(100) wafers (cut to 6×6 mm pieces) were cleaned with a modified literature method [26], widely used in the field of semiconductor technology for many years [27] to obtain fully hydrophilic surfaces. The basis is an alkaline treatment to remove organic contaminants, followed by an acidic treatment to remove inorganic contamination. A simple criterion is that the contact angle of water on the cleaned surfaces is very small, typically less than 8°. Recently, it was found that the acidic treatment cannot create totally hydrophilic surfaces (contact angle of water >20°) [28]. We found that the acidic treatment can increase the contact angle to 23° from 10° obtained in the previous alkaline step. Thus we modified the method by reversing the sequence of the acidic and alkaline treatments. In the first step, the silicon wafers were treated for 15 min at 80 °C in a mixture of concentrated hydrochloric acid (30% HCl): concentrated hydrogen peroxide (31%):water with a volume ratio of 1:1:5. In the second step, they were treated for another 15 min at 80 °C in a mixture of concentrated ammonia (25% NH_4OH): concentrated hydrogen peroxide (31%):water with a volume ratio of 1:1:5. The cleaned surfaces are completely hydrophilic with contact angles <5° (the exact value is difficult to measure and usually considered as zero in the literature) [28]. The silicon wafers are now covered by a thin and continuous layer of SiO_x (with $x \sim 2$). After drying in flowing argon, the wafers were immediately subjected to silanization. Note that we employed the same method also for borosilicate glass surfaces.

2.3. Silanization

A freshly pretreated and dried silicon wafer (or glass) substrate was placed in a mini reactor, 2 μl of pure liquid silane were cast onto the surface, and incubated for a specified period. After silanization, the sample was rinsed with absolute ethanol to remove most of the remaining silane, and ultrasonicated in absolute ethanol for 2–3 min in order to remove unwanted aggregates (if any). Next, it was rinsed with water and dried in flowing argon. The mini reactor consisted of a fluoropolymer O-ring (Viton®) placed between two flat glass plates. The small enclosed volume ensures that the silane remains liquid during the silanization process, due to its low vapor pressure. The procedure requires only very small amounts of silane (~2 μl) for sample surfaces of some tens of mm^2. All silanization processes were performed at room temperature of 26±3 °C and at ambient humidity of 26±4%.

2.4. Instrumentation

Ellipsometry was performed with an EL-X02C ellipsometer (DRE GmbH, Germany). The incidence and reflectance angles were 70°, the wavelength of the laser was 632.8 nm. A three-layer model (air/silane+SiO_2/Si) was used to calculate the thickness of the silane films, according to a literature method [29,30]. For simplicity, the refractive indices of silanes (1.45–1.5) are considered the same as that of SiO_2 (1.4571). Among the samples pretreated in one batch, the thickness error was ±0.02 nm. A piece of silicon from the same batch (~6 pieces) was taken as blank reference. Obviously, the thickness difference between the silanized sample and the reference is due to the growth of silane films.

Water was used as the probe liquid for advancing contact angle measurements. The apparatus for this purpose was a Krüss G10 contact angle goniometer. For each sample, five points were measured, and the contact angles averaged. AFM images were recorded with a Nanoscope IIIA (Digital Instruments) operated in tapping mode (280 to 300 kHz) with silicon tips.

For SFG spectroscopy we used a picosecond pulsed Nd:YAG laser (Ekspla) pumping an Optical Parametric Generation/Optical Parametric Amplifier (LaserVision) to generate infrared light tunable between 1000 and 4000 cm^{-1}. The infrared beam had an energy of 300 μJ at 3000 cm^{-1} with a bandwidth of ~6 cm^{-1}. A visible beam (532 nm) was created by second harmonic generation in a Potassium Titanyl Arsenate crystal. The angles of incidence of the infrared and visible beams were 60° and 50°, respectively, at the susbstrates, with an energy density of ~20 mJ/cm^2 and 40 mJ/cm^2, respectively [31]. Our polarization code (*e.g.* "ssp") refers to analyzer (SFG beam)/polarizer (VIS)/polarizer (IR). The sample was placed in a vacuum cell, evacuated to ~10^{-4} Pa for 1 h and backfilled with Ar. This procedure reduced the amount of surface contamination that would adsorb to the surface in the laboratory

Table 1
Ellipsometric thickness (d) and advancing contact angle (θ_a) of OTS, DTS, PTS and DPES SAMs and the silanization time (t)

	Structure	d (nm)	θ_a (°)	t (h)
DPES	$Ph_2P(CH_2)_2Si(OEt)_3$	0.56±0.06	48±1	0.2–0.5
PTS	$CH_3(CH_2)_2Si(OEt)_3$	0.47±0.06	80±2	>12
DTS	$CH_3(CH_2)_9Si(OEt)_3$	1.02±0.08	102±2	>10
OTS	$CH_3(CH_2)_{17}Si(OEt)_3$	2.33±0.11	102±2	>8

All the data herein refer to the silane films whose ellipsometric thicknesses do not further change and AFM images show no aggregates.

Table 2
Rms (root-mean-square) roughness data of AFM images in Figs. 1 and 4*

	Condition	Rms (nm)
Fig.1A	Bare Si	0.17±0.02
Fig. 1B	OTS, >8 h	0.14±0.02
Fig. 4A	OTS, 20 s	0.13±0.02
Fig. 4B	OTS, 20 min	0.16±0.02
Fig. 4C	OTS, 60 min	0.34±0.03
Fig. 4D	OTS, 120 min	0.67±0.04
Fig. 4E	OTS, 480 min	0.14±0.02

*The Z-axial range in all the AFM images is 4 nm. The value for each image is averaged from at least five individual samples.

environment. The data were acquired while the infrared energy was continuously scanned from 2750 to 3200 cm^{-1} at 1 cm^{-1}/s. Each data point in a spectrum is an average of 20 shots. The spectra presented are an average of five scans with error bars representing the standard deviation between the spectra. The spectra are curve-fitted with a Lorentzian line shape function, using non-linear fitting functions in Origin® with instrumental setting for the error bars.

3. Results and discussions

3.1. Characterization of CM–SAMs by ellipsometry, contact angle, AFM and SFG

SAMs of silanes have important applications in the fields of adhesion, lubrication, corrosion protection, and grafting nanostructures. Coverage, thickness, orientation, and purity all have a critical impact, thus it is important to gain sufficient knowledge of these properties. In this study, we achieved a comprehensive characterization by combining ellipsometry, contact angle, AFM, and SFG experiments, while each technique on its own can only reveal limited features. Note here that at least five individual samples were employed to test the reproducibility for each condition. Ellipsometry can provide a global measure for thickness of adsorbates on substrates, but it cannot differentiate between discrete islands and continuous films. Contact angles merely report the wettability. AFM demonstrates the (local) morphological quality of the film, but can usually not give any chemical information. In contrast, SFG (sum frequency generation), a modern spectroscopic method, gives the vibrational characteristics of chemical groups, plus the molecular orientation of monolayers [32,33].

Among the four triethoxysilanes studied, OTS (n-$C_{18}H_{37}Si(OEt)_3$), DTS (n-$C_{10}H_{21}Si(OEt)_3$), and PTS (n-$C_3H_7Si(OEt)_3$) have methyl end groups, but different carbon chain lengths, while DPES ($Ph_2PCH_2CH_2Si(OEt)_3$) features a PPh_2 end group. The thicknesses and contact angles of these silane films (Table 1) are qualitatively consistent with the reported values [3,25,34–36]. The small contact angle of DPES indicates its poor order (and probably low density packing), expected from its branched shape and short carbon chain. From PTS to OTS, the thickness increases from 0.47 to 2.33 nm, close to their own molecular lengths [20,21,34]. For PTS, the contact angle of 80° implies that its carbon chain is not highly ordered. In contrast, DTS and OTS show a higher value (*ca.* 102°), which points to a better ordered structure and packing, although the value is slightly lower than that of fully hydrophobic surfaces [3,35].

For DPES, clean and flat AFM topographies can be obtained only within a time window of 0.2–0.5 h. When the silanization time is longer, AFM images show numerous large aggregates, and the corresponding ellipsometric thicknesses are much larger than that of monolayers. The aggregation can be interpreted by its short carbon chain, and maybe also by the chemically reactive PPh_2 group. In contrast, OTS, DTS, and PTS require threshold times of 8, 10, and 12 h, respectively, for growth to saturation. The unusually long silanization times are assigned to the high viscosity of the neat silane liquids, which is based on strong intermolecular interactions, and probably causes low mobility/

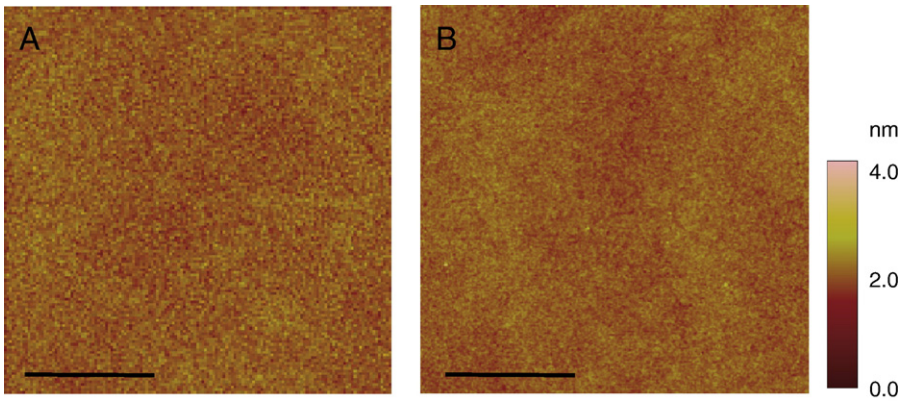

Fig. 1. Tapping mode AFM images of an oxidized silicon wafer reference (A) and an OTS-modified wafer (B). Scale bar=1 μm.

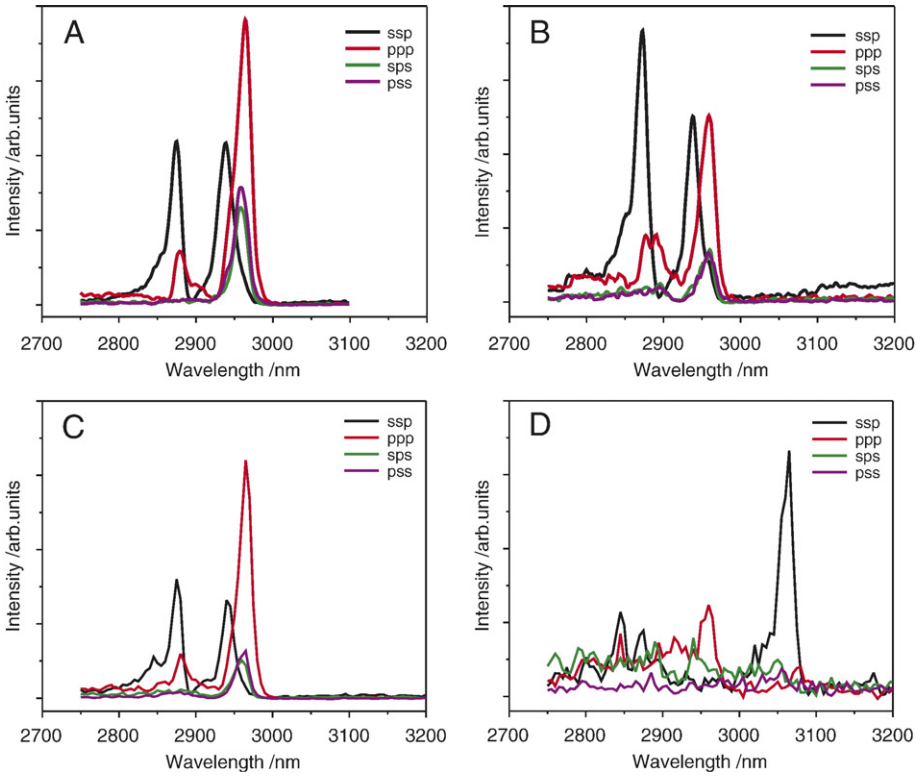

Fig. 2. Sum frequency spectra of silane monolayers on borosilicate glass at various polarization settings. A) OTS, B) PTS, C) DTS and D) DPES.

flexibility of the silanes on the substrate. The carbon chain length-dependent growth time appears to be consistent with the larger adsorption and growth rates for longer carbon chains in the case of thiols [37,38]. For longer times, no significant changes in ellipsometry, contact angle and AFM images were observed.

Since AFM images of the four silane films are simply flat and featureless (see Supporting Information), we present here only OTS as example (Fig. 1), together with a bare silicon wafer for comparison. The rms (root-mean-square) roughness values for Fig. 1A and B (each from five pieces of different samples) 0.17±0.02 nm and 0.14±0.02 nm, respectively, see Table 2. This indicates the uniformity of the silane films and the bare silicon substrates. The silanized surface was essentially free of aggregates, which consist of hydrolyzed molecules and can easily achieve heights of >3 nm [39]. Large numbers of such aggregates would change the optical parameters of the SAM and thus influence the ellipsometrically determined thicknesses, which was not observed in our case.

The mentioned characterizations verify a thin film on a silanized substrate, but yield no information on the chemical identity. We found that Fourier transform infrared (FTIR) spectroscopy in reflection mode and also in attenuated total reflection configuration suffers from low signal/noise ratios. Considering the extremely low sensitivity of a polarized IR beam reflected from a silicon wafer [40], this is not very surprising, although some results are available in the literature [41,42]. When IR spectroscopy in transmission is impossible, SFG is a very good alternative, which additionally offers extreme surface sensitivity. We tested not only silicon substrates, which have the same drawback as in FTIR experiments, but also borosilicate glass substrates. The composition on the top layer of a silicon wafer, which is actually native silicon oxide, is very similar to that of glass. The native silicon oxide layer is typically 1.5 to 2.0 nm thick, sufficient to restrict the silanization reaction to the surface. Therefore, we used glass to mimic silicon wafers in SFG studies, assuming that the monolayers are equivalent on the surface of these two different materials.

Fig. 2 shows SFG spectra of all silane films, obtained for four different polarization combinations. Several groups reported the SFG spectra for silane monolayers prepared from silane solutions [43,44]. Albeit the SFG beam was not analyzed with respect to its polarization, the VIS–IR (visible–infrared) combinations pp, ps and sp yield spectra that compare nicely with our analogues in Fig. 2 (ppp, sps, and ssp, respectively) [43,44]. The results on glass compare very well with spectra presented here: OTS with ssp polarization shows two main peaks at 2875 cm^{-1} and 2936 cm^{-1}, which correspond to ν_s (CH_3) and its Fermi resonance [45]. Smaller intensities at 2850 cm^{-1} and 2961 cm^{-1} are due to CH_2 modes and $\nu_{as}(CH_3)$, respectively. The SFG spectra here indicate an ordering that is close to that in films formed by solution methods. Further confirmation comes from the sps and pss cases: Now ν_{as} (degenerate) appears at 2958 cm^{-1}, and CH_2 resonances are not visible, again suggesting the picture of a relatively ordered film.

The PTS films prepared from solution [44] and ours show similar spectra: ssp polarization yields two main features at 2875 cm^{-1} and 2936 cm^{-1}, which correspond to $\nu_s(CH_3)$ and its Fermi resonance. $\nu_{as}(CH_3)$ and CH_2 modes show relatively small intensities. In the case of sps mode, the ν_{as} (degenerate)

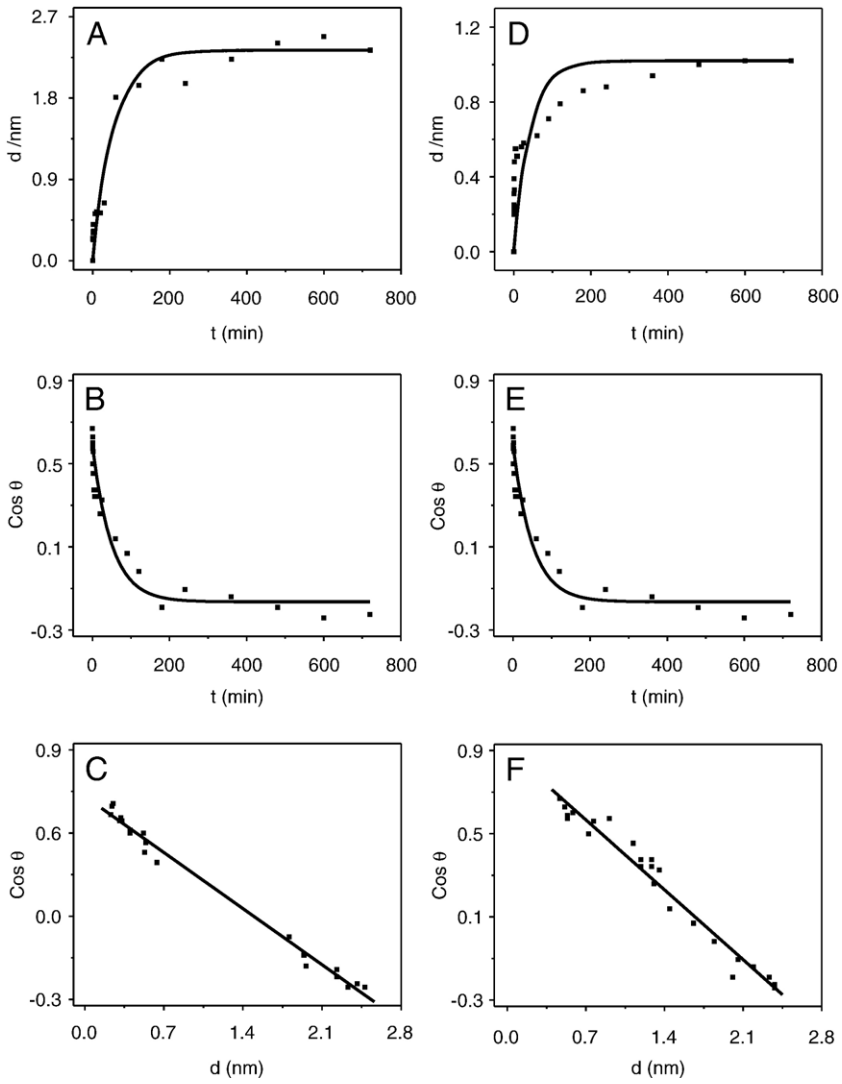

Fig. 3. Ellipsometry and contact angle measurements of OTS (A–C) and DTS (D–F) films. A and D: ellipsometric thickness *d vs.* time *t*; B and E: cosine of contact angle cosθ *vs.* time *t*; and C and F: cosine of contact angle cosθ *vs.* ellipsometric thickness *d*.

appears at 2958 cm^{-1}, while CH_2 and CH_3 display weak intensity between 2860–2880 cm^{-1}. These data indicate some order of the packing in the silane film. DTS presents, as expected, an intermediate case. Since the CH_3 resonance is comparable with the case of OTS, the DTS packing properties should be similar. DPES yields spectra that are more challenging to interpret. The weak CH_2 and CH_3 vibrations at 2950 cm^{-1} and 2875 cm^{-1} in the spectra indicate that there may be some contaminants or unreacted ethoxy groups of the silane present on the surface. This makes it difficult to justify if the weak CH_2 resonance originates from the carbon chain or from unreacted ethoxy groups; here isotopic labeling (with deuterium) would be required for unambiguous assignments. Nevertheless, the most important conclusion is the presence of a clear ν(C–H) resonance from the phenyl groups at 3064 cm^{-1}. This compares well with the case of phenylsilane on silicon [46], where ν_{7b} and ν_2 of the C–H (phenyl) vibrations were detected at 3038 cm^{-1} and 3059 cm^{-1}, respectively. It was also found that the ssp signal yields best results [46]. Hence SFG here proves the presence of the phenyl groups.

Taking all the ellipsometry, contact angle data and AFM images together, we can conclude that the silanized surfaces are nearly fully covered with a thin film of single molecular thickness of the respective silane. For PTS and DPES, the films are poorly ordered. In contrast, DTS and OTS present relatively ordered self-assembled monolayers, although of slightly inferior quality, compared to the solution method.

3.2. Growth mechanisms for OTS and DTS CM–SAMs

Only knowing how to fabricate SAMs is not sufficient, knowledge of the growth mechanisms is essential to control the quality and properties. Much effort was directed at understanding the growth mechanism in SM and VM [42,47–50]. As stated above, the CM attracted little attention [8,25], let alone its growth mechanism. In the following we show how ellipsometry, contact angle measurements and AFM complementarily provide insight on growth kinetics for the cases of OTS and DTS.

Fig. 3 shows *ex-situ* ellipsometry and contact angle measurements of OTS and DTS during assembly. In case of

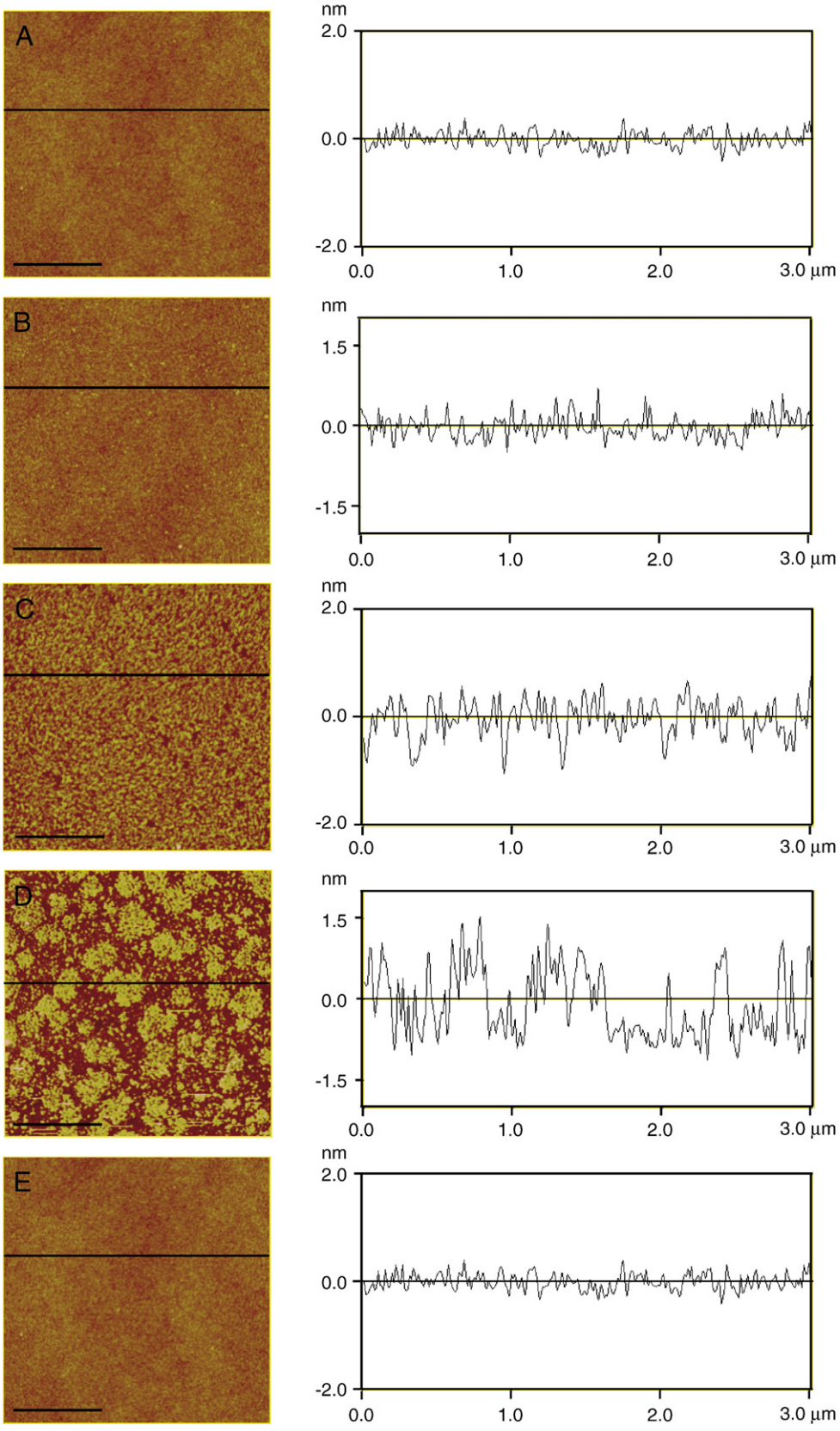

Fig. 4. Tapping mode AFM images of OTS-modified oxidized silicon surface with increasing immersion time, A) 20 s, B) 20 min, C) 60 min, D) 240 min and E) 480 min. Scale bar = 1 µm. *Z*-axial range = 4 nm.

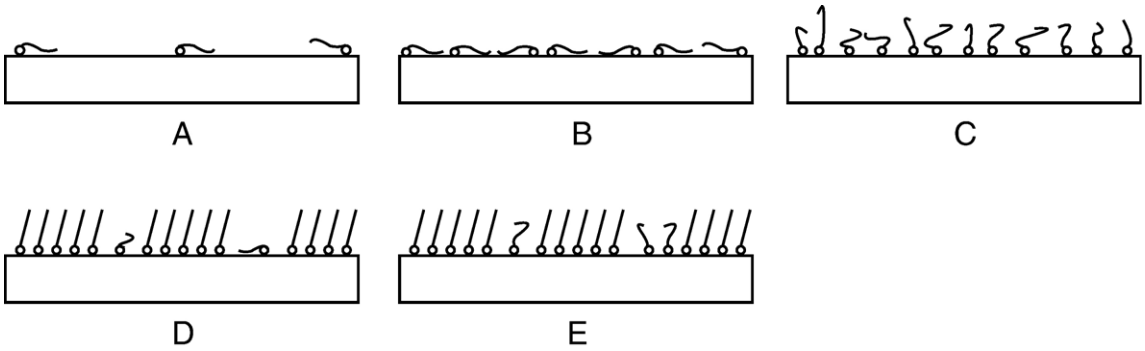

Fig. 5. Cartoons describing the growth mechanism of OTS SAMs.

OTS, both thickness (Fig. 3A) and contact angle (Fig. 3B) *vs.* silanization time approximately show a first order exponential behavior (see supporting information), which corresponds to Langmuir kinetics [47,51,52]. Clearly such a simple adsorption mechanism is only qualitative. One should also consider that, at any stage of film formation (see discussion below), one can assume a mixture of organic matter and silicon oxide on the wafer surface. Then the Cassie equation [53]

$$\cos\theta = x_1\cos\theta_1 + x_2\cos\theta_2$$

describes how the measured contact angle θ depends on the relative coverages of organic matter, x_1, and silicon oxide, x_2 (with their respective contact angles θ_i). The predicted linear relationship between $\cos\theta$ and x_1 corresponds to the linearity between $\cos\theta$ and the film thickness in Fig. 3C, since the coverage is directly proportional to the measured thickness. DTS behaves in a similar way. The slightly larger deviation from the Langmuir-like behavior may be due to additional processes such as physisorption [54].

AFM is a powerful tool to visualize the morphology of substrate surfaces and adsorbed films [48–50,55,56]. We preferred *ex-situ* AFM (and hence "quenching" of the assembly process) because we are interested in stable SAMs, covalently bound to the surface, rather than in weakly bound (physisorbed) molecules, which can easily be removed by rinsing, but might interfere with AFM.

The AFM images in Fig. 4 characterize the growth of an OTS monolayer as a function of immersion time. The rms roughness values, see Table 2, show dramatic changes from 0.13±0.02 nm (Fig. 4A), to 0.67±0.02 nm (Fig. 4D), and back to 0.14±0.02 nm (Fig. 4E). The line profiles in the right column also show a change of roughness value from small (<0.3 nm) through large (~2.3 nm) to small (~0.3 nm). The roughness analyses can be used to infer the packing properties of the SAMs [42,48]. In detail, for Fig. 4A (20 s silanization) we do not observe any distinct features, but a flat surface. Comparing Fig. 4A with Fig. 1A, and combining it with the ellipsometry (0.3 nm) and contact angle results (50°), one can verify the existence of silane molecules on the surface. However, the coverage of OTS is low, and the molecules should lie flat on the surface. After 20 min, see Fig. 4B, the surface rms roughness increases to 0.16±0.02 nm from 0.13±0.02 nm (Fig. 4A). The few tiny bright dots can be assigned to residual polycondensated aggregates [39]. Note that the distance Δh (the height difference between the apices and pits in the profiles) of 0.4 to 0.8 nm in Fig. 4A and B, is comparable with the cross section of alkylsilanes (~0.5 nm) [57]. After 60 min, a significant change of the surface morphology was observed, see Fig. 4C. The surface is overall uniform and of nearly full coverage, with Δh varying from 1.0 to 1.4 nm. The rms roughness increase to 0.34±0.03 nm, see Table 2. Since the ellipsometric thickness is (1.2±0.2) nm, we assign the dark pits to the silicon/silicon oxide substrate, on which OTS molecules might reside in *gauche* (kinked) conformations, with stretching lengths of only 1.0 to 1.4 nm.

Within the period from 60 min to 240 min, the surface changes dramatically, illustrated by the newly emerging bright patches in Fig. 4D. The rms roughness increase to 0.67± 0.04 nm. The heights of these fractal islands are 0.8–2.5 nm. If the dark areas are considered as bare substrate areas, the bright patches cannot account for the total film thickness of (1.9± 0.2) nm, found ellipsometrically. Thus the pits should be covered by silane molecules, similar to the state in Fig. 4B. Taken together, it is reasonable to assign the bright patches and dark pits to ordered and disordered domains of a SAM, respectively [42].

When the silanization time reaches 480 min (see Fig. 4E), island patches cannot be observed any more, and the OTS layer is uniform and clean The contrast between the apices and pits decreases markedly to 0.1 to 0.4 nm (Fig. 4E), which is also supported by the rms roughness value of 0.14±0.04 nm. Since there are no aggregates on the OTS film, and since the surface is fully covered, the nominal thickness is totally due to the contribution from the SAM. Comparing with Fig. 4D, we postulate that the thickness increase is mainly from changes in the dark areas, where the OTS molecules all or partially rise up (still in *gauche* conformation) from the lying-down state in the previous snapshot. After 12 h silanization, we did not observe significant differences in terms of morphology, nominal thickness and contact angle. This indicates that the molecules in *gauche* and/or lying-down conformation in the pits do not change their vertical stretching length. Non-active OH sites and confinement on the molecular level might be responsible for that.

From the above-mentioned considerations, we can outline a growth scenario for OTS SAMs, shown in Fig. 5A–E (corresponding to Fig. 4A–E). In the first stage, only small

amounts of silane molecules are anchored at the most active sites on the silicon surface. Although overall the silane/silicon oxide surface is uniform and smooth (as characterized by AFM, ellipsometry, and contact angle measurements), the local activity on the molecular scale is certainly not ubiquitously uniform. In the quasi-equilibrium 2D-phase diagram of thiol SAMs, this state is termed as vapor (V) or gas (G) phase, as the thiol molecules are very mobile on the surface [58]. In the case of silane SAMs, silane molecules are usually thought to be irreversibly anchored, *i.e.*, reactively chemisorbed [3,59,60]. However, some researchers reported that the adsorbed silane molecules are mobile and can diffuse laterally on the surface [35,61,62]. The coverage in Figs. 4A and 5A is apparently quite low and the interactions among silane molecules would be rather weak. The mobile property and the weak intermolecular interaction of these silane molecules at this stage are bit analogous to the gas molecules. Thus for simplicity, the term "gas (G) phase" is adopted to describe Fig. 5A [1]. Subsequently, Fig. 5B shows a surface completely covered with lying-down molecules. Compared to Fig. 5A, nominally, the difference is only the molecular coverage. But intrinsically, the interaction among molecules becomes significantly strong, and in turn the molecular movement remarkably confined. Thus it is termed as "liquid (L)", *correspondingly*; again, this does not simply imply surface diffusion. In the following (Fig. 5C), it appears that the lying-down molecules raise by taking on extended conformations while other molecules from the bulk silane react with surface OH groups to form a more densely packed layer. Its packing density is still well below that of a "solid phase". Thus "liquid-expanded (LE)" is coined to describe this state. Note that the nominal thickness of the LE phase can span a wide range from ca 1.0 to 2.0 nm in our case, depending on the stretching extent. With further silanization time (Fig. 5D), the LE molecules extend fully in the vertical direction, corresponding to a conformational change from gauche to all-trans. Consequently, they form highly ordered patches, termed as "liquid crystalline (LC)", comparable to condensed islands. Surrounding these islands are some gas- or liquid-like OTS molecules. Such a coexistence of two phases in the growth process of silane SAMs is well known [63–65]. If the silanization proceeds to 8 h or more, a more uniform and dense monolayer is acquired, see Figs. 4E and 5E. The remarkable change is the rising of the molecules in the dark areas where they form either an L phase or an LE phase. Longer time does not increase the film thickness significantly, indicating that the final state is a mixture of LC and LE (and/or L). Note that all the terms (G, L, LE, LC) are borrowed from the terminology of Langmuir films [1]. In analogy to such films, one can expect highly ordered layers below a certain temperature T_c, and disordered layers above T_c [65–68]. Considering the influence of kinetics, the OTS behavior can be qualitatively interpreted well in this regime [48]. Note that a similar evolution scenario was also observed in the SAMs growth of DTS (Supporting Information).

4. Conclusion

Fabrication of self-assembled monolayer films by simply casting neat silane reagents in ambient environment was demonstrated. The films were systematically studied *via* chemical and structural characterization by means of SFG, AFM, water contact angles and ellipsometry. Films with shorter carbon chains (PTS), or branched (DPES) silanes showed poor ordering. In contrast, longer carbon chain silanes (OTS and DTS) assembled to ordered monolayers. For OTS and DTS, a Langmuir-type kinetics of the film formation was revealed by time evolution studies. The film growth experienced a transition from lying-down to standing-up geometries, similar to observations for the solution method.

Supporting Information Available: AFM images of PTS, DTS and DPES; AFM images of DTS growth with time; roughness analyses of AFM images, fitting parameters for the dynamics of the ellipsometric thickness; water droplet contact angles.

References

[1] D.K. Schwartz, Annu. Rev. Phys. Chem. 52 (2001) 107.
[2] Y. Barness, O. Gershevitz, M. Sekar, C.N. Sukenik, Langmuir 16 (2000) 247.
[3] R. Maoz, J. Sagiv, D. Degenhardt, H. Möhwald, P. Quint, Supramol. Sci. 2 (1995) 9.
[4] M.J. Stevens, Langmuir 15 (1999) 2773.
[5] M.J. Pellerite, E.J. Wood, V.W. Jones, J. Phys. Chem. B 106 (2002) 4746.
[6] V. Depalma, N. Tillman, Langmuir 5 (1989) 868.
[7] H.A. Al-Abadleh, A.L. Mifflin, M.J. Musorrafiti, F.M. Geiger, J. Phys. Chem. B 109 (2005) 16852.
[8] G.A. Husseini, J. Peacock, A. Sathyapalan, L.W. Zilch, M.C. Asplund, E.T. Sevy, M.R. Linford, Langmuir 19 (2003) 5169.
[9] M.C. Henry, L.K. Wolf, M.C. Messmer, J. Phys. Chem. B 107 (2003) 2765.
[10] Y. Jin, X. Kang, Y. Song, B. Zhang, G. Cheng, S. Dong, Anal. Chem. 73 (2001) 2843.
[11] R.A. Komoroski, A.J. Magistro, P.P. Nicholas, Inorg. Chem. 25 (1986) 3917.
[12] R.G. Freeman, K.C. Grabar, K.J. Allison, R.M. Bright, J.A. Davis, A.P. Guthrie, M.B. Hommer, M.A. Jackson, P.C. Smith, D.G. Walter, M.J. Natan, Science 267 (1995) 1629.
[13] N.E. Cant, K. Critchley, H.L. Zhang, S.D. Evans, Thin Solid Films 426 (2003) 31.
[14] J.Y. Tseng, M.H. Lin, L.K. Chau, Colloids Surf., A 182 (2001) 239.
[15] N. Tillman, A. Ulman, J.S. Schildkraut, T.L. Penner, J. Am. Chem. Soc. 110 (1988) 6136.
[16] K. Keren, M. Krueger, R. Gilad, G. Ben-Yoseph, U. Sivan, E. Braun, Science 297 (2002) 72.
[17] Y.F. Ma, J.M. Zhang, G.J. Zhang, H.X. He, J. Am. Chem. Soc. 126 (2004) 7097.
[18] K. Keren, R.S. Berman, E. Buchstab, U. Sivan, E. Braun, Science 302 (2003) 1380.
[19] P. Silberzan, L. Leger, D. Ausserre, J.J. Benattar, Langmuir 7 (1991) 1647.
[20] N. Kumar, C. Maldarelli, C. Steiner, A. Couzis, Langmuir 17 (2001) 7789.
[21] M.E. McGovern, K.M.R. Kallury, M. Thompson, Langmuir 10 (1994) 3607.
[22] H. Sugimura, A. Hozumi, T. Kameyama, O. Takai, Surf. Interface Anal. 34 (2002) 550.
[23] P.W. Hoffmann, M. Stelzle, J.F. Rabolt, Langmuir 13 (1997) 1877.
[24] A. Hozumi, Y. Yokogawa, T. Kameyama, H. Sugimura, K. Hayashi, H. Shirayam, O. Takai, J. Vac. Sci. Technol., A 19 (2001) 1812.
[25] T.J. Horr, J. Ralston, R.S.C. Smart, Colloids Surf., A 97 (1995) 183.
[26] W. Kern, RCA Eng. 28 (1983) 99.
[27] D.A. Puotinen, RCA Rev. (1970) 187.
[28] J.J. Cras, C.A. Rowe-Taitt, D.A. Nivens, F.S. Ligler, Biosens. Bioelectron. 14 (1999) 683.

[29] S.R. Wasserman, G.M. Whitesides, I.M. Tidswel, B.M. Ocko, P.S. Pershan, J.D. Axe, J. Am. Chem. Soc. 111 (1989) 5852.
[30] J.D. LeGrange, J.L. Markham, Langmuir 9 (1993) 1749.
[31] S. Baldelli, J. Phys. Chem., B 107 (2003) 6148.
[32] C.Y. Wang, H. Groenzin, M.J. Shultz, J. Am. Chem. Soc. 126 (2004) 8094.
[33] S. Nihonyanagi, D. Miyamotao, S. Idojiri, K. Uosaki, J. Am. Chem. Soc. 126 (2004) 7034.
[34] S.R. Wasserman, Y.T. Tao, G.M. Whitesides, Langmuir 5 (1989) 1074.
[35] J. Foisner, A. Glaser, T. Leitner, H. Hoffmann, G. Friedbacher, Langmuir 20 (2004) 2701.
[36] M.S. Chen, S.L. Brandow, W.J. Dressick, Thin Solid Films 379 (2000) 203.
[37] L.S. Jung, C.T. Campbell, Phys. Rev. Lett. 84 (2000) 5164.
[38] S. Xu, S.J.N. Cruchon-Dupeyrat, J.C. Garno, G.Y. Liu, G.K. Jennings, T.H. Yong, P.E. Laibinis, J. Chem. Phys. 108 (1998) 5002.
[39] X.D. Xiao, G.Y. Liu, D.H. Charych, M. Salmeron, Langmuir 11 (1995) 1600.
[40] H. Brunner, U. Mayer, H. Hoffmann, Appl. Spectrosc. 51 (1997) 209.
[41] H. Hoffmann, U. Mayer, H. Brunner, A. Krischanitz, Vib. Spectrosc. 8 (1995) 151.
[42] T. Vallant, H. Brunner, U. Mayer, H. Hoffmann, T. Leitner, R. Resch, G. Friedbacher, J. Phys. Chem., B 102 (1998) 7190.
[43] P. Guyot-Sionnest, R. Superfine, J.H. Hunt, Y.R. Shen, Chem. Phys. Lett. 144 (1988) 1.
[44] J. Löbau, A. Rumphorst, K. Galla, S. Seeger, K. Wolfrum, Thin Solid Films 289 (1996) 272.
[45] R.A. MacPhail, R.G. Snyder, H.L. Strauss, J. Chem. Phys. 77 (1982) 1118.
[46] K.A. Briggman, J.C. Stephenson, W.E. Wallace, L.J. Richter, J. Phys. Chem., B 105 (2001) 2785.
[47] R. Resch, M. Grasserbauer, G. Friedbacher, T. Vallant, Appl. Surf. Sci. 140 (1999) 168.
[48] C. Carraro, O.W. Yauw, M.M. Sung, R. Maboudian, J. Phys. Chem., B 102 (1998) 4441.
[49] D.B. Asay, S.H. Kim, J. Chem. Phys. 124 (2006) 174712.
[50] H. Brunner, T. Vallant, U. Mayer, H. Hoffmann, B. Basnar, M. Vallant, G. Friedbacher, Langmuir 15 (1999) 1899.
[51] A.G. Richter, C.J. Yu, A. Datta, J. Kmetko, P. Dutta, Phys. Rev., E 61 (2000) 607.
[52] T. Vallant, J. Kattner, H. Brunner, U. Mayer, H. Hoffmann, Langmuir 15 (1999) 5339.
[53] A. Cassie, S. Baxter, Trans. Faraday Soc. 40 (1944) 546.
[54] K.A. Peterlinz, R. Georgiadis, Langmuir 12 (1996) 4731.
[55] T. Balgar, R. Bautista, N. Hartmann, E. Hasselbrink, Surf. Sci. 532–535 (2003) 963.
[56] Y. Wang, M. Lieberman, Langmuir 19 (2003) 1159.
[57] F. Schreiber, Prog. Surf. Sci. 65 (2000) 151.
[58] O. Cavalleri, H. Kind, A.M. Bittner, K. Kern, Langmuir 14 (1999) 7292.
[59] J. Sagiv, J. Am. Chem. Soc. 102 (1980) 92.
[60] A. Ulman, Chem. Rev. 96 (1996) 1533.
[61] A.N. Parikh, D. Allara, I.B. Azouz, F. Rondelez, J. Phys. Chem. 98 (1984) 7577.
[62] S. Franzka, D. Dahlhaus, N. Hartmann, Thin Solid Films 488 (2005) 124.
[63] D.K. Schwartz, S. Steinberg, J. Israelachvili, A.N. Zasadzinski, Phys. Rev. Lett. 69 (1992) 3354.
[64] K. Bierbaum, M. Grunze, A.A. Baski, L.F. Chi, W. Schrepp, H. Fuchs, Langmuir 11 (1995) 2143.
[65] M. Goldmann, J.V. Davidovits, P. Silberzan, Thin Solid Films 327–329 (1998) 166.
[66] R.R. Rye, Langmuir 13 (1997) 2588.
[67] K. Iimura, Y. Nakajima, T. Kato, Thin Solid Films 379 (2000) 230.
[68] J.B. Brzoska, I.B. Azouz, F. Rondelez, Langmuir 10 (1994) 4367.